

Redox-active heterobinuclear triazenide-bridged complexes; ancillary ligand control of electron distribution in a three-electron metal–metal bond

Neil G. Connelly,*^a Owen D. Hayward,^a Phimphaka Klangsinrikul,^a A. Guy Orpen*^a and Philip H. Rieger*^b

^a School of Chemistry, University of Bristol, Bristol, UK BS8 1TS. E-mail: Neil.Connelly@bristol.ac.uk

^b Department of Chemistry, Brown University, Rhode Island, RI 02912, USA

Received (in Basel, Switzerland) 3rd March 2000, Accepted 14th April 2000

Neutral heterobinuclear triazenide-bridged complexes are oxidised to paramagnetic monocations; the electron distribution in the σ^* metal–metal orbital of rhodium–iridium complexes may be controlled by the ancillary ligands at the two metals.

Systematic carbonyl substitution reactions^{1–3} of the redox-active $[\text{Rh}_2]^{2+}$ complex $[\text{Rh}(\text{CO})_2(\mu\text{-RNNNR})_2\text{Rh}(\text{CO})_2]$ ($\text{R} = \text{C}_6\text{H}_4\text{Me-}p$ throughout) have led to the stabilisation of the core oxidation levels $[\text{Rh}_2]^{3+}$ {e.g. in $[\text{Rh}(\text{CO})(\text{PPh}_3)(\mu\text{-RNNNR})_2\text{Rh}(\text{CO})(\text{PPh}_3)]^+$ }¹ and $[\text{Rh}_2]^{4+}$ {e.g. in $[\text{RhCl}(\text{CO})(\text{PPh}_3)(\mu\text{-RNNNR})_2\text{Rh}(\text{bipy})]^+$ ($\text{bipy} = 2,2'$ -bipyridine)}.² Moreover, detailed structural and EPR spectroscopic studies have shown the SOMO of the $[\text{Rh}_2]^{3+}$ complexes to be σ^* with respect to the Rh–Rh bond.⁴ We now describe the synthesis, characterisation and redox properties of novel heterobinuclear triazenide-bridged analogues, with RhM ($\text{M} = \text{Ir}$ or Pd) cores, and show how the electron distribution in the Rh–Ir bond of paramagnetic $[\text{RhIr}]^{3+}$ complexes is remarkably dependent on the ancillary ligands at the two linked metals.

Mixing CH_2Cl_2 solutions of the neutral triazene complexes $[\text{RhCl}(\text{CO})_2\{\text{N}(\text{H})\text{RNNNR}\}]$ [$\nu(\text{CO})$ 2095 and 2025 cm^{-1}] and $[\text{IrCl}(\eta^4\text{-cod})\{\text{N}(\text{H})\text{RNNNR}\}]$ (formed from the triazene and $[\{\text{Rh}(\mu\text{-Cl})(\text{CO})_2\}_2]$ or $[\{\text{Ir}(\mu\text{-Cl})(\eta^4\text{-cod})\}_2]$, respectively) resulted in ligand exchange to give a mixture of $[\text{IrCl}(\text{CO})_2\{\text{N}(\text{H})\text{RNNNR}\}]$ [$\nu(\text{CO})$ 2082 and 2004 cm^{-1}]⁵ and $[\text{RhCl}(\eta^4\text{-cod})\{\text{N}(\text{H})\text{RNNNR}\}]$. Subsequent addition of NEt_3 to the mixture then gave a dark red solution containing $[\text{Rh}(\eta^4\text{-cod})(\mu\text{-RNNNR})_2\text{Ir}(\text{CO})_2]$ **1** which was separated (from the homobinuclear dimer $[\text{Ir}(\text{CO})_2(\mu\text{-RNNNR})_2\text{Ir}(\text{CO})_2]$)⁵ by column chromatography (Table 1).[†] A comparison of the IR carbonyl spectrum of **1** with those of $[\text{M}(\eta^4\text{-cod})(\mu\text{-RNNNR})_2\text{M}(\text{CO})_2]$ [$\text{M} = \text{Rh}$, $\nu(\text{CO})$ 2064 vs and 2002 s; $\text{M} = \text{Ir}$, $\nu(\text{CO})$ 2049 vs and 1986 s cm^{-1}] suggested the presence of an $\text{Ir}(\text{CO})_2$ unit {rather than $\text{Rh}(\text{CO})_2$ }, supported by the observation of two doublet ¹³C resonances at δ 31.2 and 31.0 [$J(^{103}\text{Rh}^{13}\text{C})$ 15 Hz], for the pairs of inequivalent rhodium-

bound alkenic carbons of the cod ligand and confirmed by the X-ray crystal structure (Fig. 1).[‡]

Passing CO gas through a CH_2Cl_2 solution of **1** yielded $[\text{Rh}(\text{CO})_2(\mu\text{-RNNNR})_2\text{Ir}(\text{CO})_2]$ **2** which reacted with P-donor ligands to give the heterobinuclear complexes $[\text{Rh}(\text{CO})(\text{PPh}_3)(\mu\text{-RNNNR})_2\text{Ir}(\text{CO})_2]$ **3** and $[\text{Rh}(\text{CO})\text{L}(\mu\text{-RNNNR})_2\text{Ir}(\text{CO})\text{L}]$ [$\text{L} = \text{PPh}_3$ **4** or $\text{P}(\text{OMe})_3$ **5**]. A comparison of the ³¹P NMR spectra of **3** { δ 38.9 [d, $J(^{103}\text{Rh}^{31}\text{P})$ 151 Hz]} and **4** { δ 39.2 [d, $J(^{103}\text{Rh}^{31}\text{P})$ 154 Hz], 14.3, s} confirms sequential phosphine substitution at Rh and then Ir. The preference for the $\text{Ir}(\text{CO})_2$ isomers of **1** and **3** and the lower $\nu(\text{CO})$ wavenumbers for $\text{Ir}(\text{CO})_2$ than for $\text{Rh}(\text{CO})_2$ in $[\text{Rh}(\eta^4\text{-cod})(\mu\text{-RNNNR})_2\text{M}(\text{CO})_2]$ are consistent with the Ir centre being somewhat more electron rich than the Rh centre in cases such as **2**, i.e. Ir orbital energies are slightly higher than Rh, other things, such as ancillary ligands, being equal.

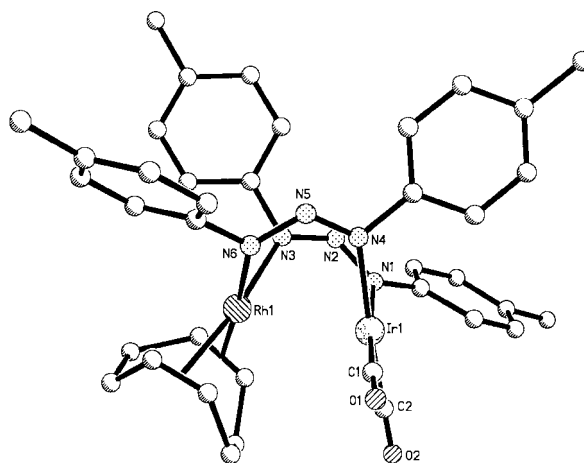


Fig. 1 Structure of **1** (H atoms omitted for clarity); Rh–Ir 2.8462(8) Å.

Table 1 IR and electrochemical data for $[\text{RhL}_m(\mu\text{-RNNNR})_2\text{M}'\text{L}'_n]^z$

Complex	L_m	$\text{M}'\text{L}'_n$	z	Yield (%)	Colour	$\nu(\text{CO})/\text{cm}^{-1}$ (in CH_2Cl_2)	E°/V^a
1	$\eta^4\text{-cod}$	$\text{Ir}(\text{CO})_2$	0	46	Dark red	2052vs, 1984s	0.53, 1.39
1⁺b	$\eta^4\text{-cod}$	$\text{Ir}(\text{CO})_2$	1	90	Dark brown	2089vs, 2040s	—
2	$(\text{CO})_2$	$\text{Ir}(\text{CO})_2$	0	82	Red–purple	2084vs, 2052m, 2019m, 1995w	0.76, 1.40(I)
3	$(\text{CO})(\text{PPh}_3)$	$\text{Ir}(\text{CO})_2$	0	81	Dark red	2049vs, 1987sh	0.43, 1.35(I)
4	$(\text{CO})(\text{PPh}_3)$	$\text{Ir}(\text{CO})(\text{PPh}_3)$	0	51	Dark red	1974s, 1953vs	0.07, 1.27
4⁺b	$(\text{CO})(\text{PPh}_3)$	$\text{Ir}(\text{CO})(\text{PPh}_3)$	1	92	Dark orange	2043s, 2011vs	—
5	$(\text{CO})\{\text{P}(\text{OMe})_3\}$	$\text{Ir}(\text{CO})\{\text{P}(\text{OMe})_3\}$	0	65	Red–purple	1992s, 1970vs	0.08, 1.09(I)
6	$(\text{CO})_2$	$\text{Pd}(\eta^3\text{-allyl})$	0	39	Orange	2071vs, 2009s	0.97
7	$(\text{CO})_2$	$\text{PdCl}(\text{PPh}_3)$	0	50	Orange–red	2075vs, 2012s	1.09, –1.31(I) ^c
8	$(\text{CO})(\text{NCMe})$	$\text{PdCl}(\text{PPh}_3)$	0	61	Brown	1983s	0.67, 1.41(I), –1.54(I) ^c

^a In CH_2Cl_2 , at a platinum electrode, with 0.1 mol dm^{-3} $[\text{NBu}_4][\text{PF}_6]$ as supporting electrolyte. For an irreversible (I) process, the oxidation peak potential, $(E_p)_{\text{ox}}$, is given at a scan rate of 200 mV s^{-1} . All potentials are relative to the saturated calomel electrode. Under the experimental conditions, E° for the one-electron oxidation of $[\text{Fe}(\eta\text{-C}_5\text{H}_5)_2]$ is 0.47 V. ^b Isolated as the $[\text{PF}_6]^-$ salt. ^c Irreversible reduction process; $(E_p)_{\text{red}}$ at a scan rate of 200 mV s^{-1} .

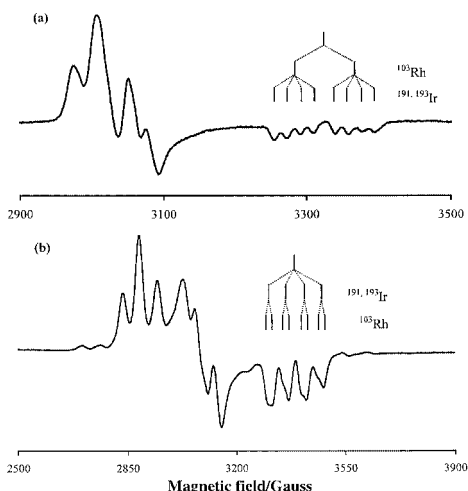


Fig. 2 EPR spectra of (a) 1^+ and (b) 4^+ at 100 K in CH_2Cl_2 -thf (1:2).

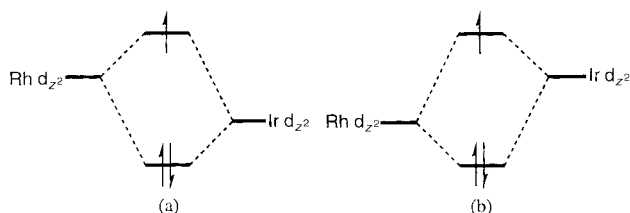
Table 2 EPR spectroscopic data^a for $[\text{RhL}_m(\mu\text{-RNNNR})_2\text{IrL}'_n]^+$

Ion	L_m	L'_n	$g_{\text{high field}}$	$A(^{103}\text{Rh})$	$A(^{191,193}\text{Ir})$
1^+	$\eta^4\text{-cod}$	$(\text{CO})_2$	2.0246(1)	82.6(2)	17.2(1)
3^+	$(\text{CO})(\text{PPh}_3)$	$(\text{CO})_2$	2.0017(1)	95.9(2)	22.3(2)
4^+	$(\text{CO})(\text{PPh}_3)$	$(\text{CO})(\text{PPh}_3)$	1.9827(1)	16.6(2)	51.6(3)
5^+	$(\text{CO})\{\text{P}(\text{OMe})_3\}$	$(\text{CO})\{\text{P}(\text{OMe})_3\}$	1.9882(4)	19.4(9)	57.4(6)

^a High field feature only; A in 10^{-4} cm^{-1} .

Cyclic voltammetry in CH_2Cl_2 shows that $1\text{--}5$ undergo two one-electron oxidation processes (Table 1) the first of which is fully reversible in all cases (the second is also reversible for 1 and 4). Treatment of the neutral complexes 1 and 4 with AgPF_6 and $[\text{Fe}(\eta\text{-C}_5\text{H}_5)_2][\text{PF}_6]$ respectively gave near quantitative yields of the paramagnetic $[\text{RhIr}]^{3+}$ -containing cations 1^+ and 4^+ (as their $[\text{PF}_6]^-$ salts). X-Ray structural studies on the redox-related pair 4 and 4^+ show a shortening of the Rh–Ir distance on oxidation, from 2.945(2) to 2.7131(9) Å, consistent with removal of an electron from a σ^* metal–metal orbital derived from the interaction of d_{z^2} orbitals, and the formation of a three-electron metal–metal bond. A similar structural difference was observed with the homobinuclear redox pair $[\text{Rh}(\text{CO})(\text{PPh}_3)(\mu\text{-RNNNR})_2\text{Rh}(\text{CO})(\text{PPh}_3)]^z$ ($z = 0$ and 1).⁴

Cations 1^+ and 4^+ , and also 3^+ and 5^+ (generated *in situ* by treatment of 3 and 5 with $[\text{Fe}(\eta\text{-C}_5\text{H}_4\text{COME})(\eta\text{-C}_5\text{H}_5)][\text{PF}_6]$ and $[\text{Fe}(\eta^5\text{-C}_5\text{H}_5)_2][\text{PF}_6]$, respectively) show well resolved EPR spectra in CH_2Cl_2 -thf (1:2); those of 1^+ and 4^+ at 100 K are shown in Fig. 2. The spectra show hyperfine coupling to ^{103}Rh ($I = 1/2$) and to $^{191,193}\text{Ir}$ ($I = 3/2$), but are complicated by Ir quadrupole coupling.⁶ The high-field g -feature is generally well resolved; the corresponding parameters are given in Table 2. These parameters clearly indicate that the distribution of unpaired electron density in the three-electron Rh–Ir bond is strongly dependent on the nature of the terminal ligands at each metal. Thus, Rh makes the major contribution to the SOMO of 1^+ and 3^+ , whereas Ir makes the major contribution in 4^+ and 5^+ .



Scheme 1 Schematic orbital interactions in the three-electron metal–metal bond of species such as (a) 1^+ and (b) 4^+ in which the ancillary ligand sets are asymmetric and symmetric, respectively.

In a first-order semi-quantitative analysis the spin density is *ca.* 75% on Ir in the species 4^+ and 5^+ in which the ancillary ligand sets at Ir and Rh are the same. When the iridium centre carries more electron withdrawing ligands (as in 1^+ and 3^+) *ca.* 80% of the spin density is located at the rhodium centre. This is consistent with the carbonyl ligands of the $\text{Ir}(\text{CO})_2$ unit reducing the Ir d_{z^2} energy below that of the Rh d_{z^2} (*i.e.* the reverse of their order in 1^+ and 3^+ , for example) leading to an inversion of the dominant contributions to the SOMO (Scheme 1). We therefore conclude that asymmetry of the ancillary ligand set can overturn the inherent metal orbital energy difference (as noted above) and reverse spin localisation in these species.

The preparative route to complexes $1\text{--}5$ can also be applied to the synthesis of redox-active rhodium–palladium complexes $[\text{Rh}(\text{CO})_2(\mu\text{-RNNNR})_2\text{PdL}_m]$ [$L_m = \eta^3\text{-allyl}$ **6**, $L_m = \text{Cl}(\text{PPh}_3)$ **7**], *i.e.* by reacting $[\text{RhCl}(\text{CO})_2\{\text{N}(\text{H})\text{RNNNR}\}]$ with $[\text{PdCl}(\eta^3\text{-allyl})\{\text{N}(\text{H})\text{RNNNR}\}]$ and $[\text{PdCl}_2(\text{PPh}_3)\{\text{N}(\text{H})\text{RNNNR}\}]$, respectively (again prepared *in situ* from the triazene and the corresponding halide-bridge dimer). Subsequent treatment of **7** with ONMe_3 in MeCN gave the highly asymmetric complex $[\text{Rh}(\text{CO})(\text{NCMe})(\mu\text{-RNNNR})_2\text{PdCl}(\text{PPh}_3)]$ **8** in which four different terminal ligands are selectively distributed between the two different metals.

In summary, the new preparative route described leads to novel redox-active heterobinuclear species which are oxidised to paramagnetic complexes in which the distribution of unpaired electron density in a metal–metal bond can be tuned by systematic ligand variation.

We thank the Royal Thai Government and the EPSRC for Studentships (to P. K. and O. D. H., respectively).

Notes and references

† All new complexes had satisfactory elemental analyses (C, H and N).
‡ X-Ray data were collected on a Siemens SMART diffractometer at 173 K for $\theta < 27.5^\circ$ with $\lambda = 0.71073$ Å. The structures were solved by direct methods and refined by least-squares against all F^2 values corrected for absorption.

Crystal data: $[\text{Rh}(\eta^4\text{-cod})(\mu\text{-RNNNR})_2\text{Ir}(\text{CO})_2] \cdot 0.14\text{CH}_2\text{Cl}_2$, $1 \cdot 0.14\text{CH}_2\text{Cl}_2$ (from CH_2Cl_2 -propan-2-ol): $\text{C}_{38.14}\text{H}_{40.28}\text{Cl}_{0.28}\text{IrN}_6\text{O}_2\text{Rh}$, $M = 919.76$, monoclinic, space group $P2_1/c$ (no. 14), $a = 15.052(4)$, $b = 13.982(2)$, $c = 17.202(3)$ Å, $\beta = 98.426(14)^\circ$, $V = 3581.3(12)$ Å³, $Z = 4$, $\mu = 4.24 \text{ mm}^{-1}$, $R1 = 0.0470$.

$[\text{Rh}(\text{CO})(\text{PPh}_3)(\mu\text{-RNNNR})_2\text{Ir}(\text{CO})(\text{PPh}_3)] \cdot 3\text{CH}_2\text{Cl}_2$, $4 \cdot 3\text{CH}_2\text{Cl}_2$ (from CH_2Cl_2 -propan-2-ol): $\text{C}_{69}\text{H}_{62}\text{Cl}_6\text{IrN}_6\text{O}_2\text{P}_2\text{Rh}$, $M = 1577.00$, triclinic, space group $P\bar{1}$ (no. 2), $a = 12.9339(5)$, $b = 15.1205(8)$, $c = 18.3009(15)$ Å, $\alpha = 83.50(4)^\circ$, $\beta = 71.74(3)^\circ$, $\gamma = 88.57(4)^\circ$, $V = 3376.7(4)$ Å³, $Z = 2$, $\mu = 2.546 \text{ mm}^{-1}$, $R1 = 0.0299$.

$[\text{Rh}(\text{CO})(\text{PPh}_3)(\mu\text{-RNNNR})_2\text{Ir}(\text{CO})(\text{PPh}_3)][\text{PF}_6] \cdot 1.5\text{CH}_2\text{Cl}_2$, $4^+[\text{PF}_6]^- \cdot 1.5\text{CH}_2\text{Cl}_2$ (from CH_2Cl_2 -*n*-hexane): $\text{C}_{67.5}\text{H}_{60}\text{Cl}_3\text{F}_6\text{IrN}_6\text{O}_2\text{P}_3$ Rh, $M = 1595.58$, triclinic, space group $P\bar{1}$ (no. 2), $a = 12.967(3)$, $b = 13.714(2)$, $c = 19.830(3)$ Å, $\alpha = 97.712(12)^\circ$, $\beta = 98.499(19)^\circ$, $\gamma = 90.430(12)^\circ$, $V = 3454.7(11)$ Å³, $Z = 2$, $\mu = 2.412 \text{ mm}^{-1}$, $R1 = 0.0640$.

CCDC 182/1602. See <http://www.rsc.org/suppdata/cc/b0/b001764g/> for crystallographic files in .cif format.

- N. G. Connelly, G. Garcia, M. Gilbert and J. S. Stirling, *J. Chem. Soc., Dalton Trans.*, 1987, 1403.
- T. Brauns, C. Carriedo, J. S. Cockayne, N. G. Connelly, G. Garcia Herbosa and A. G. Orpen, *J. Chem. Soc., Dalton Trans.*, 1989, 2049.
- N. G. Connelly, T. Einig, G. Garcia Herbosa, P. M. Hopkins, C. Mealli, A. G. Orpen, G. M. Rosair and F. Viguri, *J. Chem. Soc., Dalton Trans.*, 1994, 2025; N. G. Connelly, P. M. Hopkins, A. G. Orpen, G. M. Rosair and F. Viguri, *J. Chem. Soc., Dalton Trans.*, 1992, 2907; M. Bardaji, N. C. Brown, A. Christofides and N. G. Connelly, *J. Organomet. Chem.*, 1994, **474**, 24.
- D. C. Boyd, N. G. Connelly, G. Garcia Herbosa, M. G. Hill, K. R. Mann, C. Mealli, A. G. Orpen, K. E. Richardson and P. H. Rieger, *Inorg. Chem.*, 1994, **33**, 960.
- N. G. Connelly and G. Garcia, *J. Chem. Soc., Dalton Trans.*, 1987, 2737.
- J. A. DeGray, P. H. Rieger, N. G. Connelly and G. Garcia Herbosa, *J. Magn. Reson.*, 1990, **88**, 376.